Optimizing Mining Ventilation Using 3D Technologies

Paweł Trybała [1], Simone Rigon [1], Fabio Remondino [1], Aleksandra Banasiewicz [2], Adam Wróblewski [2], Arkadiusz Macek [2], Paulina Kujawa [2], Kinga Romańczukiewicz [2], Carlos Redondo [3], Fran Espada[3]

[1] 3D Optical Metrology (3DOM) unit, Bruno Kessler Foundation (FBK), Trento, Italy
Web: http://3dom.fbk.eu – Email: <ptrybala><srigon><remondino>@fbk.eu

[2] Department of Mining, Wrocław University of Science and Technology (WUST), Wrocław, Poland
Email: <aleksandra.banasiewicz ><adam.wroblewski><arkadiusz.macek><paulina.kujawa><kinga.romanczukiewicz>@pwr.edu.pl

[3] Hovering Solutions, Madrid, Spain - Email: <carlos.redondo><f.espada>@hoveringsolutions.com

Commission II - WG2

KEY WORDS: LiDAR, SLAM, UAV, CFD, Underground Mining

ABSTRACT:
Ventilation systems constitute an important piece of the industrial facility ecosystems. Creating proper working environmental conditions for humans is crucial, especially in hazardous sites with presence of various gases, such as underground mines. Combined with the vast amount of space to be ventilated in large mines, designing and maintaining such a system is challenging and costly. To alleviate these issues, the EIT-RM project VOT3D (Ventilation Optimizing Technology based on 3D scanning) proposes conducting advanced airflow modeling in the underground tunnel networks, utilizing computational fluid dynamics (CFD) simulations, modern surveying and 3D modeling approaches to reverse engineer a reliable geometric model of the mine and estimate the 3D airflow field inside it. In this paper, we present the challenges to be solved in this task and the proposed workflow to address them. An example related to an active industrial mine in Poland is reported as a basis for performing experimental data processing using the full, highly automatized procedure. Developments and results of underground mobile mapping (with a drone and a handheld system), point cloud processing and filtering, surface reconstruction and CFD modeling are presented. The detailed results of airflow field estimation show the advantages of the proposed solution and promise its high practical usefulness.

1. INTRODUCTION

Nowadays, ensuring employee safety in the workplace is crucial for employers. However, there are industries in which the health and safety of workers is naturally more at risk than in the others. One such industry is the underground mining. The ever-increasing demand for critical and strategic raw materials is resulting in their exploitation from lower and lower rock layers. According to Li et al. (2021), in 2021, more than 110 mines, located in the United States, Australia and Poland, were exploiting raw materials at depths of more than 1000 m below the surface. In addition, several metal mines in India, China and Canada operated at more than 2000 meters. The deepest mines, however, are in South Africa and reach depths of even more than 3000 meters below the surface - including the deepest gold mine, Mponeng, which operates at a depth of 4359 meters (Guo et al., 2022). As depth increases, so does the severeness of natural hazards - one of the main ones being the climate hazard.

The primary temperature of rock in deep underground mines is as high as over 50°C. Another factor contributing to the increase in temperature in mine workings is the work of heavy machinery, whose heated metal parts give off heat to the atmosphere (Wróblewski et al., 2021). There is also a risk associated with excavation from deep parts of the deposit, namely an increase in gas hazards. In underground mines, harmful and dangerous gases, i.e. hydrogen sulfide (H_2S), methane (CH_4), and carbon monoxide (CO), often enter the tunnels from cracks in the rock mass (He et al., 2023; Tutak et al., 2023). Those hazards are further increased by process-related gases. Many mines use diesel-powered machinery in the technological process. These engines are a source of many harmful gases, i.e. nitrogen oxides (NOx), hydrocarbons (HC), or solid particulates (Debia et al., 2017).

One of the challenges of expanding the deep excavations are the increasing distances from the mine faces to the shafts, which can reach more than 10 km. Growing tunnel network size not only directly affects the volume of space needed to be ventilated but increases the complexity of the system. This hinders the ability to predict or simulate the outcomes of introducing changes in the ventilation system. Thus, a proper ventilation system design in underground working environments is of the upmost importance for the safety and economics of mining operations.

1.1 Paper's aims

This work presents the background and driving factors of the EIT Raw Materials project VOT3D - Ventilation Optimizing Technology based on 3D scanning (https://vot-3d.com/). The project aims to address the challenges of accurate, large-scale simulation-driven design of ventilation systems. To do so, a crucial component is the proper 3D reconstruction and representation of the vast underground mining spaces.

The aim of the paper is to present the project's pipeline which embed 3D surveying, data processing and computational fluid dynamics (CFD) simulations to support the optimization of ventilation systems in underground mining.

Two dedicated mobile mapping systems are used: (i) an autonomous drone/UAV, to automatize surveys in the main parts of underground facilities and (ii) a handheld scanner, which can be deployed easily to supplement drone measurements in places inaccessible to the UAV or those featuring too complex structures. The stages of 3D data acquisition along with subsequent steps of creating and optimizing a surface mesh model for simulation purposes are showcased. CFD simulations are performed on optimized 3D surveyed data to (i) model the airflow in the underground spaces, (ii) provide the necessary information to stakeholders about possible optimization to be introduced into the ventilation system configuration and (iii) maintain the required working conditions in the mining environment. Reducing power usage of ventilation systems thanks to the proposed solution could potentially greatly decrease mining operation costs and positively affect the environmental impact.

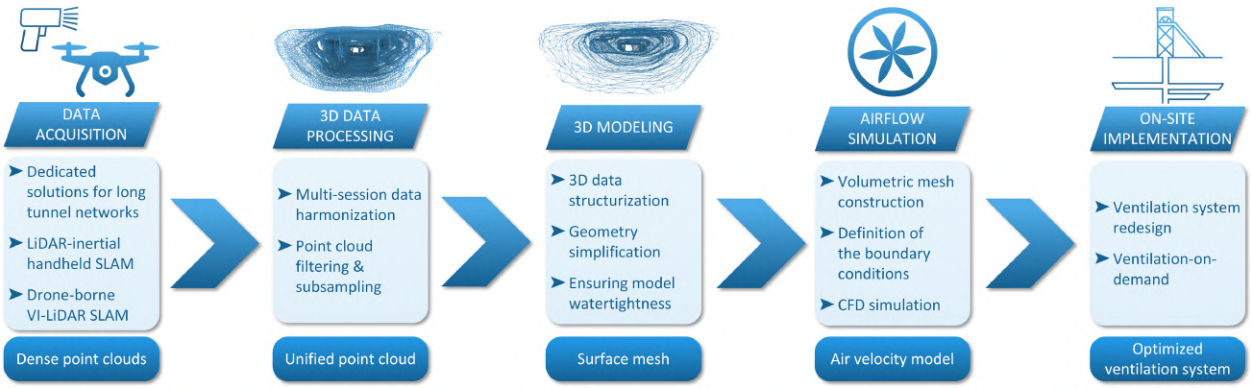

Figure 1. Ventilation system optimization workflow developed in the scope of the project.

2. VENTILATION SYSTEMS IN UNDERGROUND MINES

2.1 Requirements

The legal regulations concerning underground mine ventilation vary among the different countries around the world. This concerns the values of air quality parameters, permissible concentrations and intensities of harmful compounds and pollutants, and the method of identifying and assessing the degree of threat and preventive measures. However, the general principle of ventilation design in underground mines comes down to ensuring an appropriate amount of air of satisfactory quality in workplaces. This ensures the safety of the employees by reducing the negative impact of natural hazards, especially gas and climate hazards. European countries are implementing restrictions on the concentration values of compounds such as NOx, CO, or SO_2 through specific directives (e.g. 2017/164/EU - European Commission, 2017).

In Polish mines, concentrations required by the European Union are monitored. In addition, the national ME regulation (Regulation of Minister of Energy, 2017) prescribes the amount of oxygen at the workstation of the underground crew. The minimum amount of O_2 is 19% by volume. In Polish mines, one of the key and regulated hazards are gas and climate hazards. Coal mines are the most regulated due to the presence of methane. Copper ore mines face a hydrogen sulfide hazard and a climate hazard. As with coal and the methane hazard, the climate hazard is very extensively regulated in Polish legislation.

Not only in Poland but also in countries where underground mining is very well developed, i.e. Australia, Canada, and the USA, great emphasis is placed on proper ventilation. The most important documents regulating ventilation in underground mines in Canada are regulations issued by the Ministry of Labour (Canada Labour Code), as well as guidelines and standards developed by institutions such as Canada's Centre for Occupational Health and Safety (CCOHS) and the Mining Association of Canada (MAC).In Canada, concentrations of gases such as CO, O_2, and NO_2 are monitored overall (Schriwas & Pritchard, 2020; Rachid & Kumral, 2022). In Australia, in addition, SO_2 concentrations are also monitored at many mines. Harmful gases monitored in the US are defined by the American Conference of Governmental Industrial Hygienists in the document "Threshold Value for Substance in Workroom Air" (MSHA, 2024). In addition, air velocity monitoring is carried out in underground mines around the world - minimum velocity values and maximum values by type of underground workings are determined. System design approaches

To design a system meeting the requirements, many ventilation systems in the mines all over the world have used simplified airflow schemes, i.e., ideal geometry of the excavation. Some studies show how such a simplified model of airflow, used in a simulation, can help design a more efficient system (Maleki et al., 2018). However, the complexity of the mining tunnel network naturally suggests that the use of geometric models, more accurately represented with their 3D reconstructions, would provide much better basis of designing the ventilation network. Despite that, due to multiple challenges arising from deploying such solutions in mining conditions, no large-scale tests of such approach have been performed.

3. VOT3D SOLUTION FOR OPTIMIZING VENTILATION IN MINING

3.1 System overview

The VOT3D project proposes a novel pipeline of data processing to carry out ventilation system optimization in the industrial, underground conditions (Fig. 1). The workflow is divided into subsequent modules, thus allowing flexibility in terms of implementation in different mines. Depending on the needs of the particular facility, selected modules can be deployed alone (e.g., in case a mine already has 3D surveying data). Nevertheless, the system components were designed to work best together and provide the optimal results when used as a single, seamless workflow. The workflow components are described in detail in Section 3.2

3.2 System components

3.2.1 Autonomous measurement system

The surveying scenario of most operational underground mining facilities poses several challenges due to multiple factors:

- the environment lacks GNSS signal or any other global positioning technique;
- the lighting inside the underground site is variable and often lacking at longer tunnels;
- the low texture of the natural rock surface and presence of dust complicate visual sensors performances for position estimation and mapping;
- uneven surfaces of walls, roof and floor (which, additionally, sometimes can be partially covered by water) complicate the geometry reconstruction and prevent taking assumptions about their structure, such as presence of stable planar or linear features.

The first component of the 3D data acquisition system is an autonomous UAV developed by Hovering Solutions (Fig. 2a). The drone has been designed to minimize the influence of the abovementioned issues in the subterranean environments. Moreover, it provides a fast, agile and efficient method for data

acquisition. Although the abundant dust may affect the sensors and the presence of wind gusts (mainly caused by the ventilation system) that can reach up to 7 m/s, the platform has been proven to be able to fly autonomously in such conditions. The main objective of using autonomous robots is to reduce the risks for human operators, since the time spent in these hazardous environments can be reduced and, in most cases, it is not required for the operators to access the target area. The ability to automatize a large part of the data acquisition also enables advanced measurement scheduling for updating the 3D models with minimal effort. To be able to perform these missions, the drone carries several sensors onboard with a wide variety of technologies, offering redundancy that increases safety as well as the achieved 3D data accuracy and spatial resolution. Specifically, i) a set of image sensors pointing at different angles, ii) two inertial units thermally calibrated and a iii) set of ToF (time-of-flight) sensors using both ultrasonics and infrared working principles (both LED and laser based) are onboard, making use of a custom implementation of EKF (Extended Kalman Filter; Deilamsalehy & Havens, 2016) for the fusion of the measurements coming from each of them. Prior to the data fusion by the EKF the raw data provided by the above-described sensors is pre-processed. During this step, some data fees are correlated. For example, visual data provided by RGB sensors is matched with the information provided by the ToF sensors to solve scale uncertainties to the pure visual odometry outputs as no stereo vision is used by the robot. Inertial unit data are also used to accelerate the matching of both image features (used by the visual odometry algorithms) and the ToF spatial data matching by providing estimations prior to the next differential calculations. This fact significantly reduces the amount of processing resources (and time) required during the matching processes as algorithms are based on iterative optimizations. Data processing loop rates are normally above 50 Hz for image processing (matching and poses estimations) and between 15 and 30 Hz for ToF sensors. Each estimator provides odometry data (position and linear velocity) and its own dynamic co-variances, information that is finally fused by the EKF along with inertial unit outputs. The positions estimated obtained in this way enable robust autonomous navigation capabilities, simultaneously reconstructing the geometry of the environment at the same time. The data is processed in real-time by the central processing unit carried by the drone to allow adapting the flight plan to variations in the environment and being able to go through section changes and crossroads without any disturbance in the trajectory. The system also employes an anticollision system that ensures retaining a minimum distance to any type of obstacle. Therefore, it works as an additional safety layer, minimizing the risks of the autonomous operation.

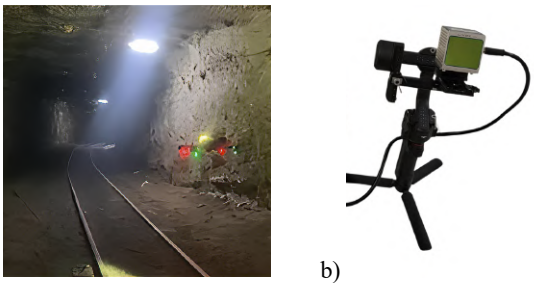

a) b)

Figure 2. Mobile laser scanning technologies deployed in the underground mine: on an autonomous UAV (a) and with the handheld PoLiMap system (b).

The second mobile mapping technique used in the project is the PoLiMap - Portable Livox-based Mapping system (Trybała et al., 2023), jointly developed by Wrocław University of Science and Technology and Bruno Kessler Foundation (Fig. 2b). The assembled system consists of a Livox Avia LiDAR sensor, mounted on a gimbal to ensure smooth movement and a secured grip, a portable power supply and a NVIDIA Jetson Xavier processing unit. The point clouds from the laser scanner and its internal inertial measurement unit (IMU) are synchronized and sent to the computing module running the Robot Operating System (ROS) for co-registration.

3.2.2 Point cloud processing

The UAV has real-time onboard computation capabilities mainly for autonomous flight purposes. For detailed mapping purposes, the raw data are stored to allow re-processing after the mission without computational limits. Using flight logs, statistical analyses of the data from each sensor are carried out and corrections are applied to reduce the inherent drift. Once the raw data from the sensors has been corrected, a localization algorithm is applied, using bundle adjustment and loop closure to improve the consistency and accuracy of the 3D data.

On the other hand, the PoLiMap data are processed in real-time within a ROS environment using FAST-LIO2 (Xu & Zhang, 2021) as the LiDAR-inertial odometry for estimating the sensor trajectory. Then, its output is integrated with a custom loop closure detection and matching module, using GTSAM-based pose graph structure to optimize the trajectory and the accumulated point cloud. Further details are reported in Trybała et al. (2023).

Finally, a custom point cloud smoothing procedure is applied to the data coming either from a drone or a handheld scanner to reduce the noise and improve the local consistency of surface reconstruction, retaining the characteristic shapes and edges. The employed algorithm is based on the guided filter, developed for 2D image processing (He et al., 2012) and adapted to the 3D domain (Han et al., 2017). Due to the large amount of points normally acquired while surveying mining tunnels, a heavily optimized and parallelized version is implemented using Numba in Python (Lam et al., 2015). The algorithm principle is based on fitting the linear model to the locations of the point neighborhoods and can be described as follows: for a given neighborhood N of point P, its covariance $\Sigma(N)$ and centroid $\bar{P}$ are calculated. Then, the covariance matrix is regularized with a tunable parameter ϵ (1):

$$\tilde{\Sigma}(N) = \Sigma(N) + \epsilon I, \tag{1}$$

where I is an identity matrix. Then, a local linear model is constructed and the position of an adjusted point P' is calculated (2-4):

$$A = \Sigma(N)\tilde{\Sigma}(N)^{-1} \tag{2}$$
$$b = \bar{P}(1 - A) \tag{3}$$
$$P' = A\,P + b \tag{4}$$

These steps are aimed at improving the subsequent pipeline stages, as the simulation environment used later on is susceptible to generating anomalous results when faced with objects of incoherent or highly irregular geometry.

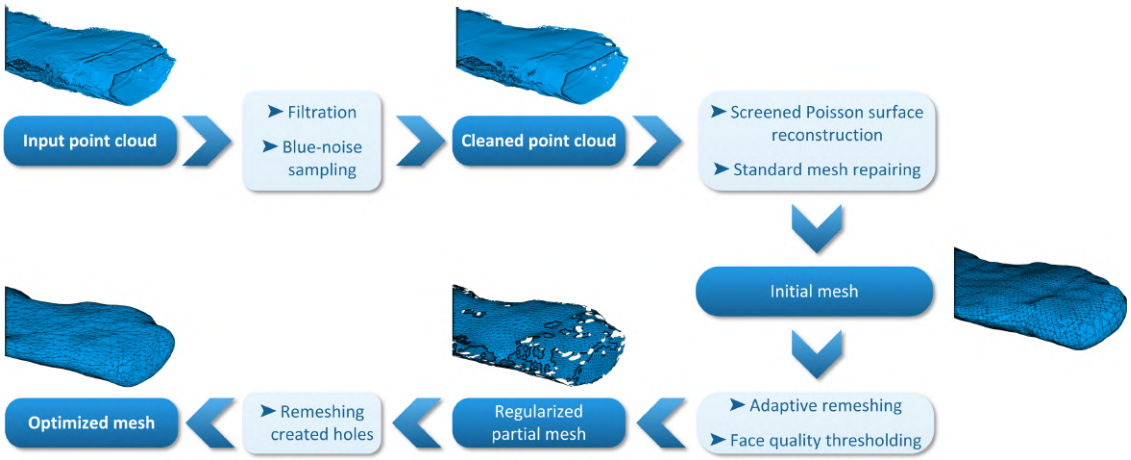

Figure 3. Meshing scheme: from the surveyed point cloud to the optimized mesh for CFD simulations.

3.2.3 3D modeling

The generated unstructured point clouds of the mining tunnels are then input into the 3D modeling workflow. A set of in-house developed Python scripts, based on open-source libraries such as Open3D (Zhou et al., 2018) or Trimesh (Dawson-Haggerty et al., 2019), handles the process of automatic creation of an optimized surface mesh model. The procedure is intended to obtain a surface tessellation, which at approximately decimeter-level accurately describes the tunnel geometry, minimizing its complexity for the following resource-demanding CFD analyses. The crucial aspects of achieving this goal are the minimization of the total face count, surface curvature and the number of triangles with acute angles.

The overview of the procedure is shown in Fig. 3. The process is defined as follows: first, the point cloud is downsampled with Poisson disk sampling (Corsini et al., 2012), which is utilized to obtain a uniform point distribution with blue noise properties on the tunnel surfaces, which improves the quality of the subsequently applied initial screened Poisson surface reconstruction (Kazhdan & Hoppe, 2013). Then, a set of modification based on the geometry of the model is applied to ensure its integrity and consistency, such as removing faces which are duplicated, degenerated or supported by few points. This surface is then regularized with adaptive remeshing (Dunyach et al., 2013). The next step filters out the triangles inflating the complexity of the mesh. The problematic, irregular elements are defined as those having their area or local curvature above their respective median values. Finally, such holes are closed with a selective screened Poisson algorithm and after ensuring the watertightness of the mode, it is passed to the next stage of processing.

3.2.4 Computational Fluid Dynamics simulation

Computational Fluid Dynamics (CFD) is based on finite volume method for numerical calculations. The method discretizes the computational domain using a volumetric mesh. Using the surface mesh obtained in the earlier stages, a volume mesh, consisting of Poly-Hexcore elements, is created. Using this meshing method, similar computational accuracy with reduced calculation time in comparison to the classical Hexcore method can be achieved (Zore et al., 2017). In order to reproduce the flow at the boundaries of the computational domain, prism layers, i.e., cell layers of thickness growing with the distance from the wall, are created (Janus, 2021). The boundary conditions, such as inlet and outlet velocities, are defined and the airflow simulation is carried out in the Ansys Fluent software.

4. EXPERIMENTAL DEMONSTRATION

4.1 Test site

To verify the proposed workflow in a real industrial environment, measurements using the autonomous UAV and the handheld PoLiMap system (Section 3.2.1) were carried out in an underground mine located in Poland. The surveyed area included a section of underground excavations extending over several kilometers. Due to the safety concerns in the conditions of the operating mine, autonomous capabilities of the drone have been heavily constrained, thus limiting the speed and the range of the UAV. Meanwhile, the PoLiMap system, together with its operator, were placed on a SUV vehicle to speed up the measurements. The UAV acquisition was performed for a 170-meter-long section, with the drone moving slowly for approximately 7 minutes. For the PoLiMap, the test survey length was approx. 1200 meters, and the sequence acquisition took 15 minutes. Although the handheld scanner allows acquiring longer sequences, especially used on a car, it still requires human physical presence, control and supervision to achieve satisfactory coverage. These downsides are minimized with the use of the aerial system, thus adding some automation capabilities of one of the most challenging parts of the workflow. Moreover, a slower measurement speed promotes achieving a higher completeness of the 3D reconstruction.

The surveyed site’s topology, together with the extent of the point cloud acquired by the drone are presented in Figure 4 whereas a top view of the PoLiMap point cloud is shown in Figure 5.

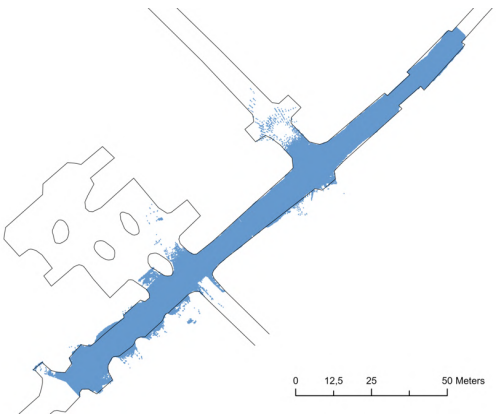

Figure 4. Top view of the tunnel network at the test site with the autonomous measurement extent (in blue).

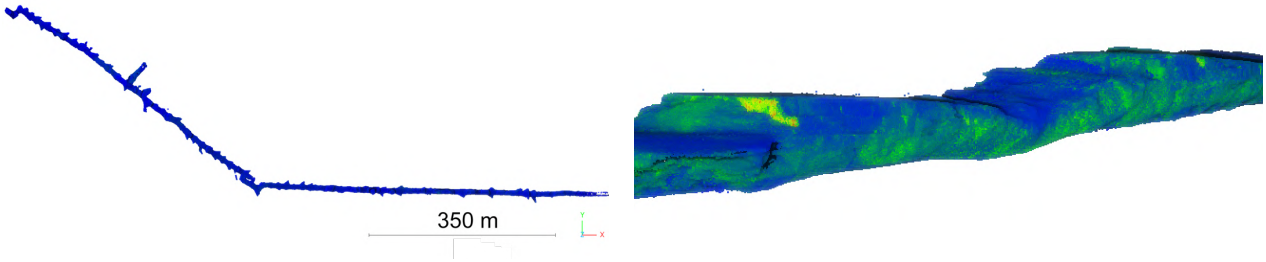

a) b)

Figure 5. Point cloud of the test site surveyed with PoLiMap: top view of the full sequence (a) and a zoom-in view from the side, showing the irregularity of the tunnel, colored by intensity (b).

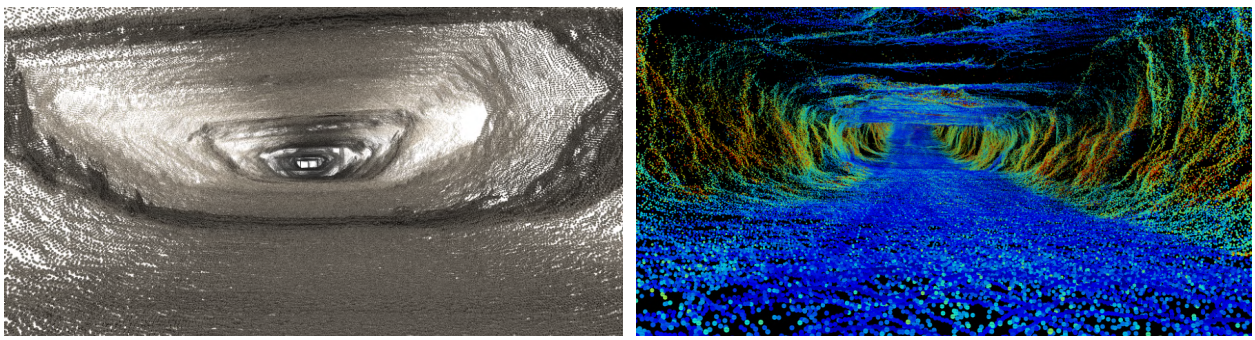

a) b)

Figure 6. Views from inside of the tunnel of the point clouds derived with the SLAM systems deployed on: autonomous aerial robot (a) and handheld PoLiMap system, colored by intensity (b).

4.2 Result

4.2.1 SLAM and point cloud filtration

The data from both mobile mapping systems were processed in the Hovering Solutions proprietary software and in the ROS environment of PoLiMap. The resulting point clouds contain 4.6 and 87.3 million points, which corresponds to average of approx. 27.000 and 73.000 points per meter (tunnel cross-section), respectively (Figure 6).

Qualitatively, the point clouds obtained by both systems correctly represented the tunnel geometry and topology, with a satisfactory degree of completeness and point density. Thus, hereafter only the point cloud acquired by the drone is used to demonstrate the capabilities of the whole data processing pipeline of VOT3D.

The point cloud was cleaned to prepare it for the meshing procedure. Outlying points were deleted using the statistical outlier filter and guided filter point cloud smoothing, with a neighborhood radius of 20 cm, was applied. The smoothing results are shown in Figure 7. The time of executing our filtering implementation was measured on a laptop with a 6-core, Intel i7-9750H @ 2.6 GHz CPU over 5 runs of the algorithm. The performance is detailed in Table 2. It can be seen that using numba greatly improves performance and parallelization brings further improvement. The difference in compilation times for the first run of the algorithm may or may not be significant, depending on the point count and the neighborhood size.

4.2.2 Surface meshing

The filtered point cloud was input into the automatic meshing procedure (Section 3.2.3). The optimized mesh is presented in Figure 8. For comparison, an initial mesh, constructed by a simple screened Poisson algorithm, was also saved. Only an additional step of ensuring its watertightness, which is a requirement of the CFD procedure, was performed. Both mesh structures are put together in Fig. 9.

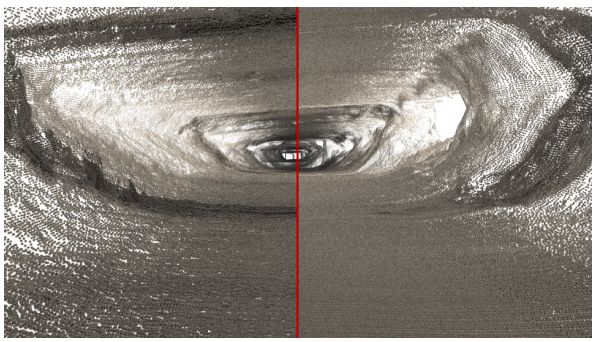

Figure 7. The point cloud acquired at the test site: raw output of SLAM (left) and the result of guided filter smoothing (right).

Implementation	Point count	Runtime [s]	
		Compilation	Smoothing
No numba	4.6 mil	-	1161.7
Numba single-threaded		6.8	232.8
Numba parallelized		10.3	74.8

Table 2. Performance statistics of the improved Python guided filter implementation.

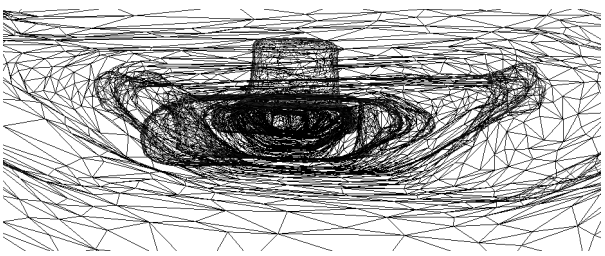

Figure 8. Resulting mesh model seen from inside of the tunnel.

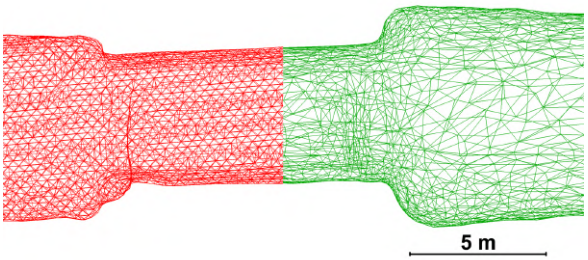

Figure 9. Resulting surface tessellations seen from the top: the initial mesh (left, in red) and the optimized mesh (right, in green)

Since the regularity of the surface elements is one of the most important factors, influencing the quality of the CFD analysis, faces of the initial and optimized mesh models were analyzed in terms of the ratio of their circumcircle and incircle radii. Quality of 100% corresponds to an equilateral triangle. The cumulative distribution of this metric (Fig. 10) shows that the optimized mesh contains less triangles of the lowest quality, which cause the most severe issues in subsequent data processing steps. Although the mean quality of the element slightly degraded from 71% to 67%, number of elements with the quality lower than 20% dropped from 7% to 3%. The optimization also allowed to decrease the number of faces from approx. 120 000 to 28 000 and increase the mean triangle area from 285 cm^2 to 1168 cm^2.

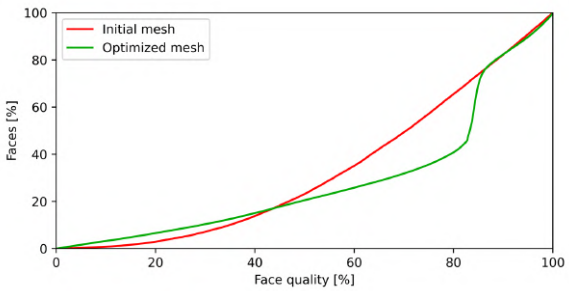

Figure 10. Comparison of surface mesh quality estimated as circumcircle/incircle radius ratio for both meshing procedures.

4.2.3 Airflow simulation

The final stage of the workflow was performed in Ansys environment, with the CFD analysis performed in Ansys Fluent. A volumetric mesh was created based on the previously prepared surface mesh. Poly-Hexcore elements were used as a base geometry of the singular cell. Their size grows from the thin inflation layers, touching the surface model, to the desired voxel resolution in the center of the tunnel. This allows to properly model the turbulent flow of air along the irregular surfaces of the tunnel. An example of the resulting cross-section through a volumetric mesh is presented in Figure 11 and the full model is visualized in Figure 12.

Finally, the airflow modeling is performed after setting the input conditions of the model (input air velocity to the system, inlet and outlet locations). Since the air velocities are estimated in a dense 3D model, for easier interpretation cross-sections are often generated. We present the example longitudinal and perpendicular to it cross-sections of the calculated airflow velocities in the tunnel in Fig. 13. A substantial variability in the velocity of the air stream can be seen, proving the need for employing such sophisticated workflow to correctly estimate the airflow velocities in the underground workings.

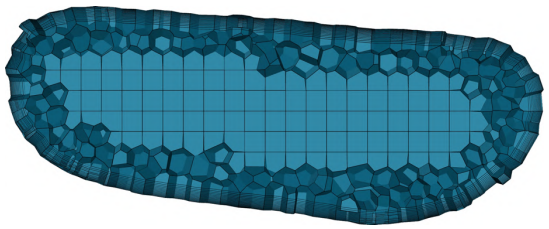

Figure 11. Cross-section through a volumetric mesh with Poly-Hexcore elements.

4.2.4 Practical outlook

The output of the CFD analysis allows the mining ventilation experts to verify the conditions in the workplace (according to the mathematical model, formulated on the basis of the realistic geometrical model of the tunnel network) and take actions to either address any issues or optimize the ventilation, adapting or redistributing its load. This could mean e.g., local addition or removal of additional fans, constraining the workers’ presence from certain areas, changing the configuration of the main fans or influencing the future development of the tunnel network. In the example used in this study, although in the examined area no prolonged presence of miners is envisioned, a potentially problematic part of the tunnel with low airflow velocity can be identified on the side of the tunnel, slightly on the right to its center (Fig. 13). Further verification of the compliance of these conditions (taking into the account also the ambient air temperature) with the regulations could lead to providing additional ventilation in this area. Such targeted strategy would limit the total cost of ensuring adherence of working conditions to the standards in terms of the ventilation network.

5. CONCLUSIONS

The paper presented the VOT3D pipeline being developed to support ventilation system optimization by using 3D technologies, like autonomous drones, handheld mobile mapping systems, 3D modeling and CFD simulations. All elements of the system were tested and showcased, acquiring and processing data in a real, currently operating underground mine in Poland.

Both mobile mapping systems proved to be effective and complementary, bringing different advantages and allowing their interchangeable use in varying conditions and scenarios. Subsequent procedures, developed for VOT3D, such as point cloud smoothing and automatized surface mesh creation and optimization, significantly improved the 3D results in their respective parts of the 3D reconstruction workflow of the mining tunnel, additionally increasing the automatization level of the process. Finally, the solution developed in the scope of the project attained expected and easily interpretable results, demonstrating to be a promising approach. Future studies will focus on the scalability of the system and further experimental verification of the results.

ACKNOWLEDGEMENTS

This work has been supported by the EIT-RM project VOT3D - Ventilation Optimizing Technology based on 3D scanning (https://vot-3d.com).

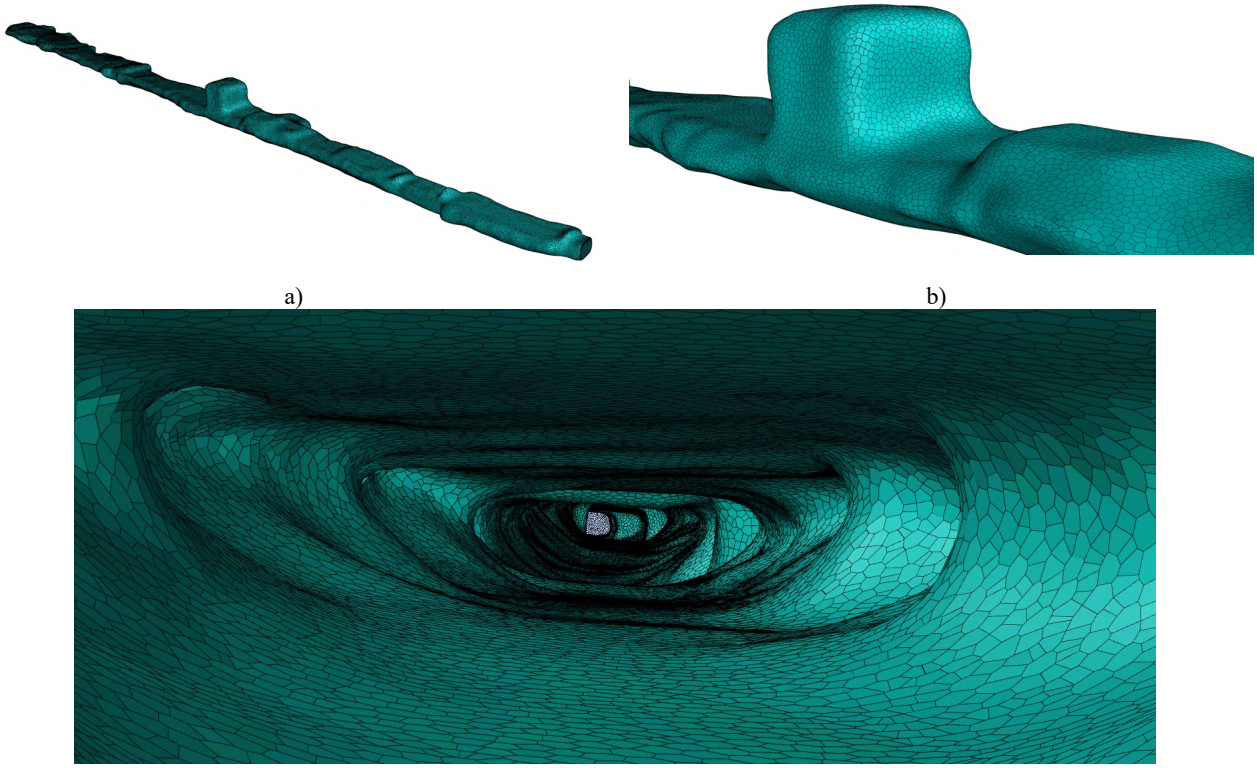

a) b)

c)

Figure 12. The volumetric mesh model with poly-hexcore elements: full test tunnel (a), zoom-in into its surface (b) and a view of the boundary elements from inside (c).

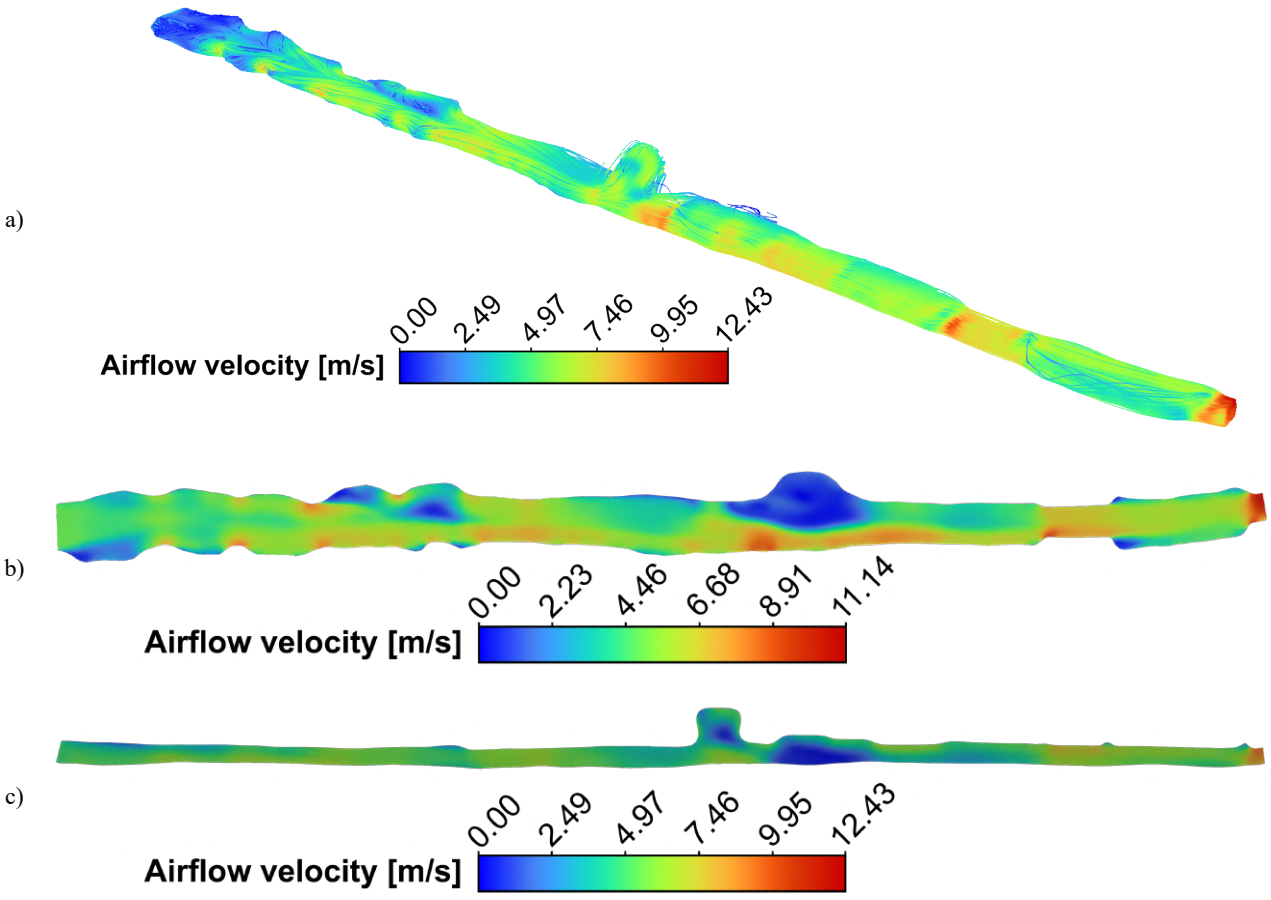

Figure 13. CFD simulation results of the airflow modeling in the test tunnel: simulated airflow pathways (a), planar (b) and longitudinal (c) sections.

REFERENCES

Corsini, M., Cignoni, P., & Scopigno, R., 2012. Efficient and flexible sampling with blue noise properties of triangular meshes. IEEE transactions on visualization and computer graphics, 18(6), p. 914-924.

Dawson-Haggerty, M. et al., 2019. Trimesh. Available online: https://trimesh.org [last access 28 April 2024].

Debia, M., Couture, C., Njanga, P. E., Neesham-Grenon, E., Lachapelle, G., Coulombe, H., Hallé, S., & Aubin, S., 2017. Diesel engine exhaust exposures in two underground mines. International Journal of Mining Science and Technology, 27(4), 641-645.

Deilamsalehy, H., & Havens, T. C., 2016. Sensor fused three-dimensional localization using IMU, camera and LiDAR, IEEE SENSORS, Orlando, FL, USA, 30.10-3.11.2016, pp. 1-3.

Dunyach, M., Vanderhaeghe, D., Barthe, L., & Botsch, M., 2013. Adaptive remeshing for real-time mesh deformation. In Eurographics 2013 - Short Papers, pp. 29–32.

European Comission, 2017. Commission Directive (EU) 2017/164 of 31 January 2017 Establishing a Fourth List of Indicative Occupational Exposure Limit Values Pursuant to Council Directive 98/24/EC, and Amending Commission Directives 91/322/EEC, 2000/39/EC and 2009/161/EU.

Guo, Q., Xi, X., Yang, S., & Cai, M., 2022. Technology strategies to achieve carbon peak and carbon neutrality for China's metal mines. International Journal of Minerals, Metallurgy and Materials, 29(4), 626-634.

Han, X.-F., Jin, J. S., Wang, M.-J., & Jiang, W., 2017. Guided 3D point cloud filtering. Multimedia Tools and Applications, 77(13), 17397–17411.

He, K., Sun, J., & Tang, X., 2012. Guided image filtering. IEEE transactions on pattern analysis and machine intelligence, 35(6), 1397-1409.

He, T., Wang, W., He, B. G., & Chen, J., 2023. Review on Optical Fiber Sensors for Hazardous-gas Monitoring in Mines and Tunnels. IEEE Transactions on Instrumentation and Measurement, vol. 72, pp. 1-22.

Janus, J., 2021. Air flow modelling on the geometry reflecting the actual shape of the longwall area and goafs. Archives of Mining Sciences, 66(4), 495-509.

Kazhdan, M., & Hoppe, H. 2013. Screened Poisson surface reconstruction. ACM Transactions on Graphics (ToG), 32(3), 1-13.

Lam, S. K., Pitrou, A., & Seibert, S., 2015. Numba: A LLVM-based Python JIT compiler. In: Proceedings of the Second Workshop on the LLVM Compiler Infrastructure in HPC, 1-6.

Li, P., & Cai, M. F., 2021. Challenges and new insights for exploitation of deep underground metal mineral resources. Trans. Nonferrous Met. Soc. China, 31(3478), 3505.

Maleki, S., Sotoudeh, F., & Sereshki, F., 2018. Application of VENTSIM 3D and mathematical programming to optimize underground mine ventilation network: A case study. Journal of Mining and Environment, 9(3), 741-752.

MSHA. 30CFR§75.322 Harmful quantity of noxious gasses, Available from https://www.law.cornell.edu/cfr/text/30/75.322 [last access 28 April 2024].

Rachid, H., Kumral, M., 2022. Addressing specific safety and occupational health challenges for the Canadian mines located in remote areas where extreme weather conditions dominate. Journal of Sustainable Mining 21.

Regulation of the Minister of Energy Related to Operations of Underground Mining (available in Polish: Rozporzadzenie Ministra Energii z dnia 23 listopada 2016 r., w sprawie szczegółowych wymagań dotyczacych prowadzenia ruchu podziemnych zakładów górniczych (Dz. U. Z 2017r.,Poz. 1118) (2017)

Shriwas, M., Pritchard, C., 2020. Ventilation Monitoring and Control in Mines. Mining, Metallurgy & Exploration 37, 1015–1021. Tran-Valade T, & Allen C., 2013. Ventilation-on-demand key consideration for the business case. Canadian Institute of Mining Convention, 5-8.05.2013, Toronto, Canada.

Trybała, P., Kujawa, P., Romańczukiewicz, K., Szrek, A., & Remondino, F., 2023. Designing and Evaluating a Portable LiDAR-based SLAM System. The International Archives of the Photogrammetry, Remote Sensing and Spatial Information Sciences, XLVIII-1/W3-2023, 191–198.

Tutak, M., Brodny, J., Małkowski, P., & Grebski, W., 2023. Applying Model Studies to Support the Monitoring of Methane Hazard during the Process of Underground Coal Mining. Production Engineering Archives, 29(3), 319-327.

Wróblewski, A., Banasiewicz, A., & Gola, S., 2021. Heat balance determination methods for mining areas in underground mines-A review. IOP Conference Series: Earth and Environmental Science, 942(1), 012011.

Xu, W., & Zhang, F., 2021. Fast-lio: A fast, robust lidar-inertial odometry package by tightly-coupled iterated kalman filter. IEEE Robotics and Automation Letters, 6(2), pp. 3317-3324.

Zhou, Q.-Y., Jaesik P., & Vladlen, K., 2018. Open3D: A Modern Library for 3D Data Processing. arXiv:1801.09847.

Zore, K., Sasanapuri, B., Parkhi, G., & Varghese, A., 2019. Ansys mosaic poly-hexcore mesh for high-lift aircraft configuration. 21th Annual CFD Symposium, 8-9.08.2019, Bangalore, India, pp. 1-11.